Structure and Electronic Properties of *In Situ* Synthesized Single-Layer MoS_2 on a Gold Surface

Signe G. Sørensen, Henrik G. Füchtbauer, Anders K. Tuxen, Alex S. Walton, and Jeppe V. Lauritsen*

Interdisciplinary Nanoscience Center, Aarhus University, DK-8000 Aarhus C, Denmark

ABSTRACT When transition metal sulfides such as MoS_2 are present in the single-layer form, the electronic properties change in fundamental ways, enabling them to be used, *e.g.*, in two-dimensional semiconductor electronics, optoelectronics, and light harvesting. The change is related to a subtle modification of the band structure due to confinement in the direction perpendicular to the sheets, and there is a considerable interest in understanding how this modification can be controlled and adjusted to generate 2D-materials with functional properties. In this article we report a synthesis procedure together with scanning tunneling microscopy and X-ray photoelectron spectroscopy characterization of two-dimensional single-layer islands of MoS_2 synthesized directly on a gold single crystal substrate. Thanks to a periodic modulation of the atom stacking induced by the lattice mismatch, we observe a structural buckling of the MoS_2 layer resulting in a characteristic moiré pattern. X-ray photoelectron spectroscopy indicates that the system develops the characteristics of n-doped MoS_2 due to electron donation. Scanning tunneling spectroscopy furthermore reflects a convolution of MoS_2 and Au donor states where the MoS_2 band structure appears modified at the band gap edges. This electronic effect is further modulated by the moiré periodicity and leads to small substrate-induced electronic perturbations near the conduction band minimum in the band gap of MoS_2. The results may be highly relevant in the context of nanopatterned two-dimensional materials on metal surfaces, and we propose the MoS_2/Au system in this article as a promising candidate to further explore the properties of supported 2D transition-metal dichalcogenides.

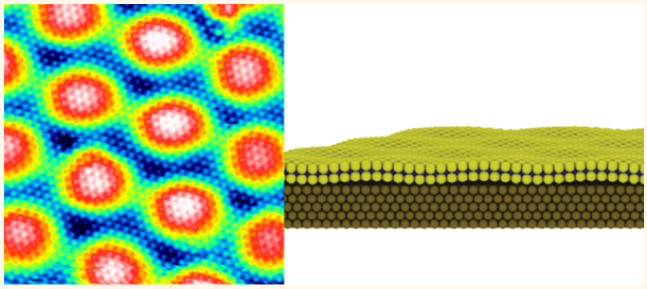

KEYWORDS: single-layer MoS_2 · monolayer MoS_2 · transitionmetal dichalcogenides · two-dimensional materials · scanning tunneling microscopy · scanning tunneling spectroscopy

Molybdenum disulfide (MoS_2) is a layered material that, in the same way as graphene, can exist as stable two-dimensional sheets consisting of single layers (or monolayers). These single layers are chemically rather inert and consist of closed-packed Mo hexagonal layers sandwiched in between two S layers in a trigonal prismatic S−Mo−S configuration. Industrial developments of MoS_2-related materials have traditionally been focused on dry lubrication applications[1] and on the hydrodesulfurization catalyst (one of the top-three most produced heterogeneous catalysts), where MoS_2 promoted with Co (so-called Co−Mo−S) acts as a catalyst for the production of low-sulfur diesel fuels.[2] More recently it has been realized that when MoS_2 is made in the single-layer form, new and intriguing properties arise with a wide range of potential uses. The main reason for this is that the electronic properties of MoS_2 are thickness dependent; *i.e.*, MoS_2 transforms from an in direct band gap semiconductor with a 1.3 eV gap into a unique 2D-material with a larger direct band gap in the single-layer form.[3−6] This property has spurred an intense interest in MoS_2 as a novel material in field-effect transistors, photodetectors, logic circuits and optoelectronic devices,[7,8] and the strong spin-splitting at the valence-band maximum makes it feasible to exploit MoS_2 in spin- and valleytronics.[9,10] Good quality MoS_2 can be produced by exfoliation from a bulk material, but synthesis of flawless extended 2D-MoS_2, which may be a prerequisite for its technological use, remains a challenge.[8,11] Recent results have shown that chemical vapor deposition

* Address correspondence to jvang@inano.au.dk.

Received for review February 18, 2014 and accepted June 17, 2014.

Published online June 17, 2014
10.1021/nn502812n

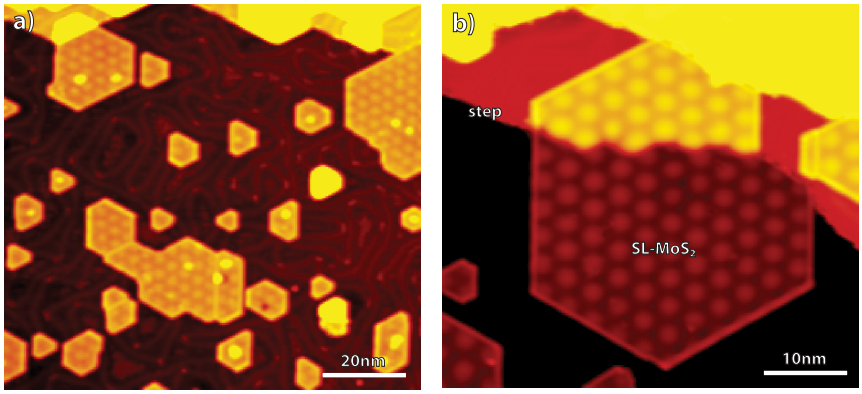

Figure 1. (a) Large-scale (100 × 100 nm) STM image of MoS_2 single-layer islands on the Au(111) surface corresponding to a surface coverage of 0.33 ML (b) 50 nm × 50 nm STM image of a single MoS_2 island with a hexagon shape crossing a single Au(111) step ($V = -1250$ mV, $I_t = 0.61$ nA).

(CVD) grown MoS_2 can be produced, but compared to mechanically produced MoS_2, the electronic properties seem to be affected by a range of defects and imperfection induced by the growth conditions.[11−13] On the other hand, naturally occurring defects have been proposed in theoretical work to be able to tweak the properties of MoS_2 in a constructive way by introducing new magnetic, electronic and optical properties.[14−16] In the same spirit, it has recently been proposed that strain may induce changes to the electronic[17] and magnetic properties[18,19] and an intense exploration of various nanostructured MoS_2 configurations, the effect of metallic dopants and grain boundaries is taking place.[8] For graphene, the fundamental exploration of such modified materials' properties has benefitted tremendously from "surface science" experiments performed on graphene synthesized by dehydrogenation of ethylene on noble metals, *e.g.*, graphene/Ir(111).[20,21] The main advantage is that advanced surface science methods, such as photoemission spectroscopy and scanning probe microscopy, can be used.[22−24] This has allowed for enormous activity in the field and a systematic approach to evaluate the effect of defects, substrate effects, chemical effects and electronic structure modulations due to substrate and adsorbate interactions.[25] A similar systematic surface science approach for analysis of single-layer MoS_2 is clearly advantageous to fundamentally address the atomic-scale properties of MoS_2 as well as offering a model system for the systematic investigation of, *e.g.*, defects, promoters and morphology effects. In addition, from both a technological and synthesis point of view, it is important to learn more about the interaction with potential substrates and metal contact points[13,17,25−29] and their potential effect on the properties of pristine MoS_2.

In this article we explore the structural and electronic properties of single-layer MoS_2 synthesized on a single-crystal Au(111) surface by means of atom-resolved room-temperature scanning tunneling microscopy (STM) and spectroscopy (STS) and X-ray photoelectron spectroscopy (XPS). The present work is inspired by a series of STM studies focused on elucidating the structure and catalytic properties of the edges of single-layer MoS_2 nanocrystallites, which is the only part of MoS_2 with an affinity for chemical interactions. The edges were shown to be reconstructed structurally and electronically compared to the bulk and were furthermore shown to be sensitive to Co, Ni, and Fe incorporation as dopants as well as dependent on the actual size of the single-layer MoS_2 particle.[14,30−33] Significantly larger MoS_2 structures are in focus in this paper, and we focus on the chemically inert MoS_2(0001) plane and its interaction with the Au(111) surface. We reveal that the lattice mismatch between MoS_2 and the gold substrate leads to an in-commensurate MoS_2 superstructure with a periodic buckling of the sheets (moiré pattern). Synchrotron-based XPS analysis shows that the chemical state of the supported MoS_2 sheets appears similar to bulk MoS_2, but the S peak is broadened and peaks are shifted to lower energies indicating that the MoS_2 becomes electron doped by the gold. The scanning tunneling spectroscopic investigation primarily shows evidence of Au interactions at the band gap edges of MoS_2 and reveals that the MoS_2 electronic structure also adopts a periodic modulation, which could be caused by local variations in the strain perpendicular to the sheets and a local variation in the direct interaction with the Au surface underneath the MoS_2.

RESULTS AND DISCUSSION

Figure 1a is a large-scale STM image of the single-layer MoS_2 islands on the Au(111) surface. The MoS_2 single-layer islands are synthesized in an ultrahigh vacuum (UHV) chamber on a pristine Au(111) surface. The MoS_2 synthesis begins with physical vapor deposition of metallic Mo from an electron-beam evaporator until the desired coverage is reached. Importantly, the evaporation of Mo is carried out in a 10^{-6} mbar H_2S atmosphere kept during the whole synthesis in order to presulfide Mo and keep it from forming an alloy with Au.

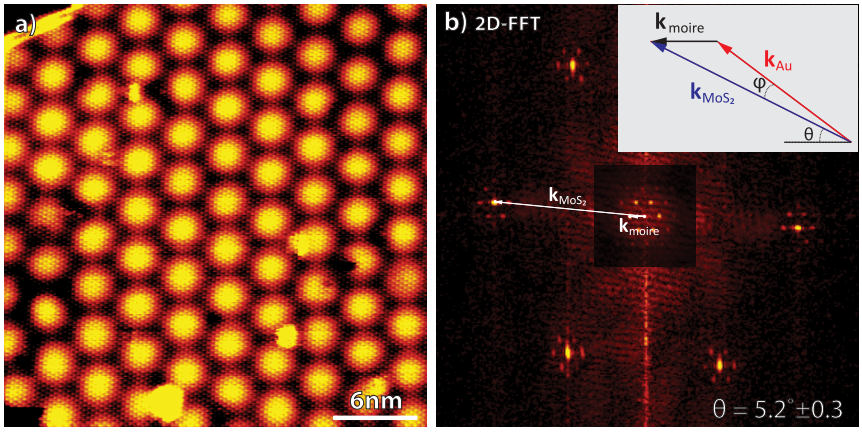

Figure 2. (a) 30 × 30 nm STM image of an extended uniform MoS_2 single-layer sheet on the Au(111) surface ($V = -1250$ mV, $I_t = 0.61$ nA) resolving both the atomic structure and the incommensurate moiré superstructure. (b) 2D fast Fourier transform (FFT) of the STM image of the extended MoS_2 sheet. For clarity the outer spots pertaining to the atomic lattice are shown with an enhanced color scale. The angle between the main reflections from the atomic lattice is $\theta = 5.2 \pm 0.3°$ relative to the moiré superstructure. The inset shows the connection between superstructure, substrate (Au) and overlayer (MoS_2) reciprocal lattice vectors.

Subsequently the MoS_2 islands are formed by post-annealing the Mo-deposited sample at 873 K for 15 min in the H_2S atmosphere. The synthesis temperature is crucial for the formation of large (>10−50 nm) MoS_2 islands. At a lower temperature of the postannealing step (673−723 K) preferentially small 3−5 nm wide MoS_2 nanocrystallites are produced, which is a result of the lower mobility of Mo. Even lower temperatures lead to incomplete sulfidation. On the other hand, higher temperatures than 873 K lead to accelerated alloying between the Mo and Au[34] at the maximum partial pressures of H_2S used in our experiments and therefore inhibits the formation of the growth of MoS_2 on the surface. The individual MoS_2 islands in Figure 1a are clearly identified by their well-defined shapes reflecting predominantly truncated triangular to hexagonal islands and vary in size from 10 nm up to more than 50 nm in width. The total area of the MoS_2 islands covers about 0.33 monolayer (ML) of the surface in this experiment. This coverage gave the most homogeneous and defect-free islands suitable for STM analysis here. Higher total coverages up to 0.7 ML could be realized by increasing the amount of deposited Mo on the surface, but this led to smaller average islands size and generation of less perfect MoS_2 structures under the present synthesis conditions. An image of an almost perfectly hexagonal MoS_2 island which is overlaid on a Au(111) step edge is illustrated in Figure 1b. A strong characteristic of the MoS_2 single-layers seen in both images of Figure 1 is the periodic buckling observed as a hexagonal set of protrusions on the (0001) basal plane of the MoS_2 islands. The hexagonal lattice is a moiré pattern that arises due to the lattice mismatch between MoS_2 and Au(111). The overlayer is incommensurate with respect to the Au(111) lattice, but the orientation and periodicity can be mathematically derived from the mismatch of the MoS_2(0001) and Au(111) lattices and the rotation, as follows.[35]

Atomic Model and Moiré Lattice. Figure 2a is an atom-resolved STM image of the atomic lattice of MoS_2 and the moiré superstructure on a single island. Figure 2b is a 2D fast Fourier transform (FFT) of the STM image that can be used to accurately determine rotations and periodicities since it represents the reciprocal space vectors present for the structure. The short-distance atomic lattice consisting of a hexagonal arrangement of protrusions seen in Figure 2a reflects an interatomic distance of 0.315 nm in all symmetry directions, which is fully consistent with the crystal structure of an unstrained, free MoS_2(0001) plane. With this value, the nominal lattice mismatch between the hexagonal lattices of MoS_2(0001) and Au(111) is 9.3%. The in-plane periodicity of the superimposed larger hexagonal superstructure in Figure 2a is measured to be 3.28 nm. As illustrated in the FFT image, the superstructure spots (closest to the origin) are slightly rotated with regard to the close packed lines of the MoS_2 lattice at an angle of $\theta = 5.2°$. This angle and the superstructure periodicity is representative of all MoS_2 single-layer islands observed in the experiment showing that a fixed epitaxial relationship is present for the MoS_2/Au(111) system.

To elucidate the epitaxial relation, we perform the following analysis of the moiré superstructure. The moiré superstructure is related to the substrate and overlayer reciprocal lattice vectors by $\mathbf{k}_{moiré} = \mathbf{k}_{MoS_2} - \mathbf{k}_{Au}$, where the magnitude of the reciprocal lattice vectors are given by $k_i = 4\pi/\sqrt{3}a_i$ and a_i are the real space lattice distances for the superstructure, MoS_2 overlayer and Au(111) substrate, respectively. The corresponding vectors are sketched in the inset of Figure 2b, where the angle θ denotes the rotation of $\mathbf{k}_{MoS_2}$ relative to $\mathbf{k}_{moiré}$ and φ is the rotation of the $\mathbf{k}_{MoS_2}$ relative to the substrate $\mathbf{k}_{Au}$ (angles are exaggerated in the inset for clarity). Using standard trigonometric

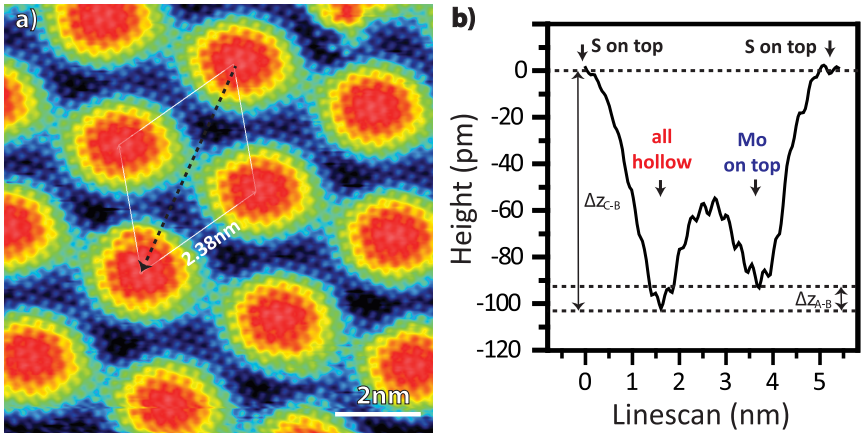

Figure 3. (a) Atom-resolved STM image of the atomic lattice and moiré superstructure of MoS_2/Au(111) ($V = -517$ mV, $I_t = 0.88$ nA). The multicolored contrast reflects higher z values in the following order: black-blue-green-yellow-red-white. (b) Linescan along the diagonal of the rhombic unit cell of the moiré superstructure showing the vertical displacement of the MoS_2 lattice.

relationships for the inset in Figure 2b with $a_{MoS_2} = 0.315$ nm, $a_{Au} = 0.288$ nm, $a_{moiré} = 3.28$ nm and $\theta = 5.2°$, a $\varphi \approx 0.45°$ rotation of the overlayer relative to the Au(111) is obtained; *i.e.*, the MoS_2 closed packed rows are very close to being perfectly aligned with the Au(111) closed packed directions. This is consistent with atom-resolved STM images of smaller islands (not shown) where both lattices are resolved, which show a nearly perfect alignment between the hexagonal S lattice and the adjacent Au(111) substrate. For the larger ensembles of islands we observed islands with both rotations $\theta = \pm 5.2°$, reflecting the simple fact that the MoS_2 layer can be rotated by $\varphi = \pm 0.45°$ at random. We note that in the above calculation we use the bulk value of 0.288 nm for the interatomic distances in Au(111) plane. This is an approximation since Au(111) in its clean state has a periodically contracted surface distance leading to the so-called herringbone surface reconstruction[36] seen as the bright ridges on the exposed Au surface in Figure 1a, which reflect a ~20 pm outward displacement of the Au atoms in this region. Since the herringbone ridges are not visible on the basal plane of the MoS_2 island itself, they seem to terminate at their perimeter or avoid the islands, which strongly suggests that the Au(111) surface is not contracted and bulk-terminated underneath the MoS_2 islands.

The linescan performed on the zoomed-in atom-resolved STM image of the MoS_2 island in Figure 3 reveals the out-of-plane corrugations associated with the formation of the moiré superstructure. The strongest corrugation seen across a superstructure unit cell (Figure 3b) is measured to be Δz_{C-B} ~100 pm, *i.e.*, a rather modest overall structural perturbation of the planar MoS_2 sheet. The modulation of height is explained by consideration of the ball model of the superstructure illustrated in Figure 4, which is constructed from the exact lattice parameters and rotation

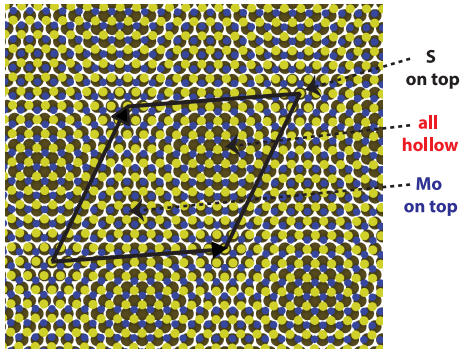

Figure 4. Top-view of a ball model of the moiré superstructure of a MoS_2 sheet on Au(111). The model assumes a 0.45° rotation between the high symmetry direction of the Au(111) and MoS_2(0001) hexagonal lattices. Mo: blue, S: yellow, Au: brown.

observed in the experiment. The placement of the MoS_2 sheet on the hexagonal Au(111) lattice is seen to generate a modulated stacking reflecting three principally different stacking domains within the superstructure unit cell: (A) S in Au *fcc* hollow sites and Mo on top of the Au atoms, (B) with both Mo and S placed near *fcc* hollow sites and finally (C) with the bottom S on-top. The existence of such three distinctly different domains within a single rhombic unit cell is directly visible in the atom-resolved image in Figure 3a. It is not *a priori* possible to identify these domains from the STM data alone due to the possibility of electronic states contributing to the STM contrast,[37−39] but given the S−Mo−S sandwich structure of MoS_2 with van der Waals bonding between the lower layer of S and the Au, the most intuitive model explains the bright domains as those with S placed on top Au (see Figure 4). In the two other domains the S are placed in hollow sites allowing for a closer average distance of the sheet toward the Au. The linescan in Figure 3b actually reveals a small difference between the two

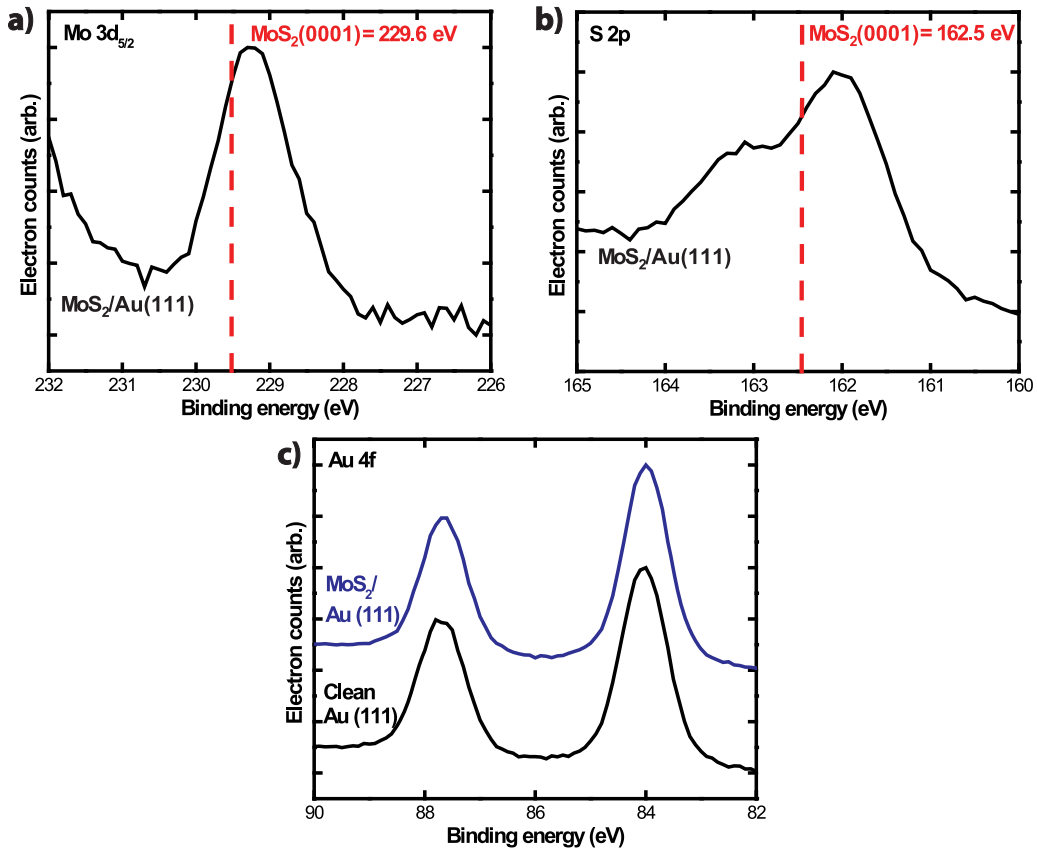

Figure 5. Core-level XPS spectra of single-layer MoS_2 islands supported on Au(111). (a) Mo $3d_{5/2}$ peak (photon energy 340 eV). Red line is reference form XPS studies of single-crystal MoS_2(0001).[40] (b) S 2p peak (photon energy 220 eV). Red line is S 2p reference form the same XPS studies as in (a). (c) Au 4f peaks (photon energy 140 eV) of clean Au(111) sample (black) and MoS_2 on Au(111) (blue).

dark domains. One domain is slightly lower by Δz_{A-B} ~10 pm, possibly reflecting the situation where neither Mo nor S is directly on-top Au allowing for a minimum distance between the sheet and the Au surface. The Δz_{C-B} and Δz_{A-B} corrugations (Figure 3b) of the moiré are only moderately sensitive to the tunneling bias in the experiment, and we did not observe contrast reversal of the moiré, which could otherwise be indicative of electronic effects.[23] We also note that the contrast difference between the two dark domains was sensitive to the STM tip-state, with values corresponding to almost no Δz_{A-B} contrast up to 40 pm observed in our experiments.

X-ray Photoelectron Spectroscopy of Single-Layer MoS_2/Au(111). To shed further light on the bonding nature and charge transfer effects contained in the MoS_2/Au(111) system we performed synchrotron-based XPS. Figure 5 shows the Mo $3d_{5/2}$, S 2p and Au 4f peaks from a freshly synthesized sample corresponding to a ~0.2 ML MoS_2 island coverage on Au(111). The Mo $3d_{5/2}$ (Figure 5a) and S 2p spectra (Figure 5b) of MoS_2/Au(111) closely resemble spectra of the single crystal MoS_2(0001), with the important difference that the Mo 3d peak at ~229.3 eV shows a small decrease in binding energy of 0.3 eV when compared to the literature value for single crystal MoS_2(0001) (229.6 eV).[40] The S $2p_{3/2}$ peak at ~162.1 eV shows a similar downshift of 0.4 eV from its bulk value (162.5 eV), although the peak is significantly broadened compared to bulk MoS_2(0001) references, where the S 2p doublet structure is normally well resolved.[40] The shift in the Mo $3d_{5/2}$ peak and S 2p position to lower binding energies is interesting since it reflects electron donation to the MoS_2 sheets from the gold. The observed electron donation is fully consistent with previous XPS studies of the inverted system, Au evaporated on MoS_2(0001),[41,42] and in accordance with the observation that MoS_2 in contact with gold behaves as an *n*-type semiconductor.[43,44] It is noted that the broadening of the S 2p spectrum indicates the presence of S in different environments,[45] which in the present case could be expected to be due to S in the upper layer of the S−Mo−S sandwich and the S toward the Au(111) surface. A comparison of the Au 4f peaks (Figure 5c), one taken on a clean Au surface and the other on the MoS_2/Au(111) system, can be used to analyze the presence of Au−S bonds. Both spectra were recorded at a photon energy of 140 eV to ensure maximum surface sensitivity toward Au. The spectra show no significant changes in peak shape, which should otherwise be present on the high binding energy side of the

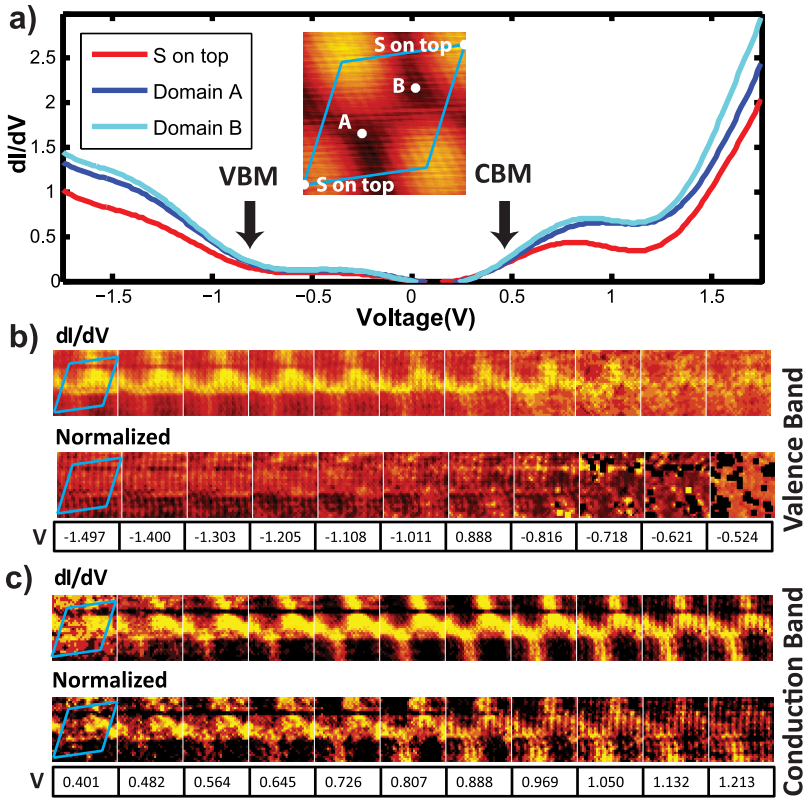

Figure 6. (a) STS graphs of the MoS_2/Au(111) system recorded in the three different domains of the STM image insert. The graph plots the d*I*/d*V* value from an average of all measurements in each domain. (b) STS images (32 × 32 pixels) as a function of bias near the valence band maximum (VBM) for the area shown in (a). The upper panel shows d*I*/d*V* values and the lower panel the d*I*/d*V* normalized by the *I*/*V*. For clarity, the contrast has been adapted in each STS image to show the variation between domains. (c) STS images as a function of bias near the conduction band minimum (CBM).

Au 4f peaks in S−Au bonded systems such as thiol overlayers on Au(111).[46] Overall, the XPS analysis therefore points to a weak interaction with no signs of direct S−Au bond formation and it therefore suggests that MoS_2 basal plane adhesion is still governed by weak van der Waals interactions. DFT studies point out that stronger interactions with Au may be expected at the MoS_2 edges under some conditions.[5,47]

Scanning Tunneling Spectroscopy on MoS_2/Au(111). To further investigate the electronic structure of the MoS_2/Au(111) system we have performed room-temperature STS on the MoS_2 islands. Figure 6a is a graph comparing d*I*/d*V*-curves recorded in a region around the center of each of the three domains of the MoS_2 superstructure (see positions in the STM insert in Figure 6a). The d*I*/d*V* curves represent to a first approximation the value of the local-density of states (LDOS) as a function of energy near the Fermi level, and variations in these curves among the different sites reflect variations in the electronic structure of the combined MoS_2/Au(111) system.[48] In all three d*I*/d*V* data sets in Figure 6a, we do not observe a full band gap corresponding to d*I*/d*V* = 0 over an extended energy range as expected for isolated bulk semiconducting MoS_2. Instead there is a region of low LDOS from approximately −0.8 to +0.5 eV, which we associate with the band gap expected for single-layer MoS_2. The structures at the low and high end of this energy range are attributed to the LDOS for energies near the valence band maximum (VBM) and conduction band minimum (CBM), respectively (see arrows on Figure 6a). The estimated band gap is then lower than the predicted ∼1.8 eV for an isolated single-layer MoS_2 sheet and 2.15 eV measured with STS for single-layer MoS_2 on HOPG.[49] The observed nonzero LDOS within the gap region and reduced apparent band gap size is likely due to Au donor states probed in STS and a contribution from direct tunneling to the Au surface. The restrictions imposed by room-temperature broadening in our experiment does not allow us to conclude further on the nature of Au donor states, but we note that previous DFT studies for an epitaxial MoS_2/Au(111) system by Bollinger *et al.*[5,14] showed that MoS_2 states near the valence band and Au states mix and gives rise to new states at the valence band edge of the combined MoS_2/Au(111) system. The donor states will have weight inside the band gap at room temperature, also at the Fermi level, and therefore the MoS_2 slab becomes slightly metallic on Au(111).

In the MoS_2/Au(111) system, the Mo and S orbital overlap to the Au surface perpendicular to the MoS_2 trilayer is modulated by the superstructure. Notably, Mo is closer to the Au surface in both the hollow and Mo on-top domains in Figure 4, and by spatially resolved STS we indeed observe that the electronic structure is slightly changed in these regions compared to the S on-top region. It is seen from the experimental d*I*/d*V* curves in Figure 6a that the LDOS in the three domains follow a qualitatively similar path, but there is a noticeable difference between the dark domains in the topography (denoted A and B) reflecting the "Mo on top" and "all hollow" domains compared with the "S on-top" domain, which exhibits a lower d*I*/d*V* in the region near the CBM. The effect is more clearly seen in the STS maps provided in Figure 6b and 6c, where the spatial distribution of the STS signal for an area covering a full unit cell is plotted as a function of bias near the VB minimum (Figure 6b) and CB maximum (Figure 6c). Regions outside these bias intervals did not show any contrast. The STS maps in Figure 6b and 6c reflect both the d*I*/d*V* and the normalized (d*I*/d*V* over *I*/*V*) signal, where the latter serves to eliminate the effect of bias-dependence on the tunneling matrix element, and it thus gives a more accurate estimate of the LDOS away from the Fermi level.[48,50] In the normalized d*I*/d*V* images in Figure 6c it is seen that the LDOS takes on a relatively higher value (bright yellow area) for the "Mo on top" and "all hollow" domains compared to the S on-top domain in the region near the CB minimum from +0.4 to +0.8 eV. The effect seems to be equally strong for both domains A and B, which cannot be discriminated in the STS data. A similar variation is not visible for the corresponding normalized d*I*/d*V* images reflecting energies around the VBM, which shows that the main effect in on the states near the CBM. The observed differences in the LDOS indicate that the interaction from the Au is influenced by the modulated distance between the Mo inside the sandwich and the Au atoms underneath. More specifically, when Mo is closer to the Au surface in the "all hollow" and "Mo on-top" domains, it is likely that stronger out-of-plane orbital overlap lead to the changed LDOS as experimentally seen near the CBM in the STS data. Moreover, we speculate slight variations in the local strain of the MoS_2 induced by the by periodic buckling perpendicular to the layer within the domains could play a role.[18,19] A future theoretical analysis of this interesting and important system could shed more light on the nature of the MoS_2 bonding to metallic substrates.

CONCLUSIONS

In conclusion, we have characterized the structure of MoS_2 islands grown as an incommensurate layer on top of a single-crystal Au(111) substrate. The lattice mismatch leads to a small out-of-plane buckling of the geometric structure reflected by a moiré superstructure with a 3.28 nm periodicity fixed by the lattice mismatch and small rotation of the MoS_2 overlayer. From the XPS analysis it is concluded that the MoS_2 single layers on Au(111) retain structural and chemical properties of MoS_2, but the XPS data and tunneling spectroscopy indicate that the interaction with Au leads to modification of the apparent band gap size and an *n*-type conductivity of MoS_2 when in contact with Au. The structural modulation also leads to a periodic variation of the electronic structure, possibly due to strain effects or variation in the out-of-plane orbital overlap between the MoS_2 sheet and the Au surface.

The MoS_2/Au(111) system presented here is a promising candidate for further studies of the fundamental properties of single-layer MoS_2 islands in heteroepixatial contact with a metal and as a method to investigate new properties that may arise due to the emergence of the superstructure and the associated modification of the band structure.[25] When synthesized under the conditions in the present paper, it is possible to study both the structure and electric properties of interfaces between MoS_2 sheets due to the coalescing of neighboring islands (Figure 1a). In successive studies, it will be highly attractive to form more uniformly and fully covered surfaces. This should be possible since, as illustrated in Figure 2b, the MoS_2 sheets are coherent over Au(111) step edges. Experimental restrictions related to the corrosive nature of H_2S at elevated pressures prevented the synthesis of a fully MoS_2 covered Au surface in our STM setup, due to the competition between the sulfide phase and Mo−Au alloy formation at elevated temperature. We expect, however, that the alloy formation can be strongly suppressed and deposition in a more concentrated H_2S atmosphere could be a future route to the formation of a MoS_2 sheet covering the entire surface. Likewise, the inclusion of electronic or structural dopants in the MoS_2(0001) lattice is highly attractive and could be systematically investigated by the synthesis method used here and a codeposition scheme previously developed for studies of promoted MoS_2 catalysts.[15,51]

METHODS

The experiments were performed in a standard ultrahigh vacuum (UHV) system equipped with a home-built Aarhus STM. The gold surface was prepared by 1.5 KeV Ar^+ sputtering followed by annealing at 900 K for 15 min, which generated an atomically clean surface exposing the herringbone reconstruction. Mo was deposited from an e-beam evaporator (EGCO4, Oxford Applied Instruments) with a deposition rate of ~0.02 monolayers/min.

H_2S with a nominal purity of 99.8% was dosed from a lecture bottle. To avoid the use of a Cu-sealed UHV leak valve, the H_2S gas was admitted from a high pressure reservoir to the vacuum through a controlled leak consisting of a ~3 cm long hollow (40 μm) glass fiber. To increase the local pressure around the sample a doser consisting of a stainless steel pipe was used to direct the H_2S onto the sample. Scanning tunneling microscopy was performed in the constant current mode. Scanning tunneling spectroscopy (STS) was performed by measuring a set of I_t (tunneling current) *vs* V (bias of sample relative to tip) curves on a 32 × 32 pixel grid covering the superstructure unit cell. Several sets of data were recorded to check for consistency and rule out the effect of localized tip-states contributing to the signal. The $I-V$ curves were then fitted and the dI/dV plotted as the derivative of the fitted graph. The value for the color contrast in the STS images was constructed from the specific dI/dV and dI/dV divided by I/V values, respectively, in each of the 32 × 32 pixels as a function of V. The image contrast was individually adjusted to show the relative variation among the domains for each image.

XPS analysis was performed at the SX-700 beamline at the ASTRID synchrotron in Aarhus, Denmark. The electron analyzer was a VG CLAM II, working with 30 eV pass energy. The MoS_2 was synthesized directly at the beamline endstation on the same Au(111) single crystal using the same Mo evaporator and H_2S dosing equipment. The coverage was estimated from comparison with XPS data for a presynthesized sample with a known coverage in STM. The binding energy was calibrated individually for each spectrum by measuring a Au 4f reference spectrum at the same photon energy (340 eV for Mo 3d and 220 eV for S 2p) and calibrating both spectra such that Au $4f_{7/2}$ = 84.0 eV.

Conflict of Interest: The authors declare no competing financial interest.

Acknowledgment. We thank J. Miwa, S. Ulstrup and P. Hofmann for fruitful discussions. J.V.L. acknowledges support from Haldor Topsøe A/S, the European Research Council (ERC Grant No. 239834 (OxideSynergy)) and The Danish Council for Strategic Research (CAT-C). We also acknowledge the Nordforsk network "An interdisciplinary approach to atomistic design of new catalysts". We acknowledge beamtime received on the SX-700 beamline at ASTRID (Aarhus, Denmark) and the help from Z. Li, Centre for Storage Ring Facilities (ISA).

REFERENCES AND NOTES

1. Tenne, R. Inorganic Nanotubes and Fullerene-Like Nanoparticles. *Nat. Nanotechnol.* **2006**, *1*, 103–111.
2. Topsøe, H.; Clausen, B. S.; Massoth, F. E. *Hydrotreating Catalysis*; Springer Verlag: Berlin-Heidelberg, 1996; Vol. 11, p 459.
3. Splendiani, A.; Sun, L.; Zhang, Y. B.; Li, T. S.; Kim, J.; Chim, C. Y.; Galli, G.; Wang, F. Emerging Photoluminescence in Monolayer MoS_2. *Nano Lett.* **2010**, *10*, 1271–1275.
4. Mak, K. F.; Lee, C.; Hone, J.; Shan, J.; Heinz, T. F. Atomically Thin MoS_2: A New Direct-Gap Semiconductor. *Phys. Rev. Lett.* **2010**, *105*, 4.
5. Bollinger, M. V.; Jacobsen, K. W.; Nørskov, J. K. Atomic and Electronic Structure of MoS_2 Nanoparticles. *Phys. Rev. B: Condens. Matter Mater. Phys.* **2003**, *67*, 085410.
6. Li, T. S.; Galli, G. L. Electronic Properties of MoS_2 Nanoparticles. *J. Phys. Chem. C* **2007**, *111*, 16192–16196.
7. Radisavljevic, B.; Radenovic, A.; Brivio, J.; Giacometti, V.; Kis, A. Single-Layer MoS_2 Transistors. *Nat. Nanotechnol.* **2011**, *6*, 147–150.
8. Chhowalla, M.; Shin, H. S.; Eda, G.; Li, L. J.; Loh, K. P.; Zhang, H. The Chemistry of Two-Dimensional Layered Transition Metal Dichalcogenide Nanosheets. *Nat. Chem.* **2013**, *5*, 263–275.
9. Mak, K. F.; He, K. L.; Shan, J.; Heinz, T. F. Control of Valley Polarization in Monolayer MoS_2 by Optical Helicity. *Nat. Nanotechnol.* **2012**, *7*, 494–498.
10. Mak, K. F.; He, K. L.; Lee, C.; Lee, G. H.; Hone, J.; Heinz, T. F.; Shan, J. Tightly Bound Trions in Monolayer MoS_2. *Nat. Mater.* **2013**, *12*, 207–211.
11. Zhou, W.; Zou, X. L.; Najmaei, S.; Liu, Z.; Shi, Y. M.; Kong, J.; Lou, J.; Ajayan, P. M.; Yakobson, B. I.; Idrobo, J. C. Intrinsic Structural Defects in Monolayer Molybdenum Disulfide. *Nano Lett.* **2013**, *13*, 2615–2622.
12. Najmaei, S.; Liu, Z.; Zhou, W.; Zou, X. L.; Shi, G.; Lei, S. D.; Yakobson, B. I.; Idrobo, J. C.; Ajayan, P. M.; Lou, J. Vapour Phase Growth and Grain Boundary Structure of Molybdenum Disulphide Atomic Layers. *Nat. Mater.* **2013**, *12*, 754–759.
13. Mann, J.; Sun, D. Z.; Ma, Q.; Chen, J. R.; Preciado, E.; Ohta, T.; Diaconescu, B.; Yamaguchi, K.; Tran, T.; Wurch, M.; *et al.* Facile Growth of Monolayer MoS_2 Film Areas on SiO_2. *Eur. Phys. J. B* **2013**, *86*, 226.
14. Bollinger, M. V.; Lauritsen, J. V.; Jacobsen, K. W.; Nørskov, J. K.; Helveg, S.; Besenbacher, F. One-Dimensional Metallic Edge States in MoS_2. *Phys. Rev. Lett.* **2001**, *87*, 196803.
15. Lauritsen, J. V.; Kibsgaard, J.; Olesen, G. H.; Moses, P. G.; Hinnemann, B.; Helveg, S.; Nørskov, J. K.; Clausen, B. S.; Topsøe, H.; Lægsgaard, E.; *et al.* Location and Coordination of Promoter Atoms in Co- and Ni-Promoted MoS_2-Based Hydrotreating Catalysts. *J. Catal.* **2007**, *240*, 218–231.
16. Zhang, Z.; Zou, X.; Crespi, V. H.; Yakobson, B. I. Intrinsic Magnetism of Grain Boundaries in Two-Dimensional Metal Dichalcogenides. *ACS Nano* **2013**, *7*, 10475–10481.
17. Fu, D. Y.; Zhou, J.; Tongay, S.; Liu, K.; Fan, W.; Liu, T. J. K.; Wu, J. Q. Mechanically Modulated Tunneling Resistance in Monolayer MoS_2. *Appl. Phys. Lett.* **2013**, *103*, 183105.
18. Shi, H. L.; Pan, H.; Zhang, Y. W.; Yakobson, B. I. Quasiparticle Band Structures and Optical Properties of Strained Monolayer MoS_2 and WS_2. *Phys. Rev. B: Condens. Matter Mater. Phys.* **2013**, *87*, 155304.
19. Chang, C. H.; Fan, X. F.; Lin, S. H.; Kuo, J. L. Orbital Analysis of Electronic Structure and Phonon Dispersion in MoS_2, $MoSe_2$, WS_2, and WSe_2 Monolayers under Strain. *Phys. Rev. B: Condens. Matter Mater. Phys.* **2013**, *88*, 195420.
20. Wintterlin, J.; Bocquet, M. L. Graphene on Metal Surfaces. *Surf. Sci.* **2009**, *603*, 1841–1852.
21. Coraux, J.; N'Diaye, A. T.; Busse, C.; Michely, T. Structural Coherency of Graphene on Ir(111). *Nano Lett.* **2008**, *8*, 565–570.
22. Balog, R.; Jorgensen, B.; Nilsson, L.; Andersen, M.; Rienks, E.; Bianchi, M.; Fanetti, M.; Lægsgaard, E.; Baraldi, A.; Lizzit, S.; *et al.* Bandgap Opening in Graphene Induced by Patterned Hydrogen Adsorption. *Nat. Mater.* **2010**, *9*, 315–319.
23. Borca, B.; Barja, S.; Garnica, M.; Minniti, M.; Politano, A.; Rodriguez-Garcia, J. M.; Hinarejos, J. J.; Farias, D.; de Parga, A. L. V.; Miranda, R. Electronic and Geometric Corrugation of Periodically Rippled, Self-Nanostructured Graphene Epitaxially Grown on Ru(0001). *New J. Phys.* **2010**, *12*, 093018.
24. Morgenstern, M. Scanning Tunneling Microscopy and Spectroscopy of Graphene on Insulating Substrates. *Phys. Status Solidi B* **2011**, *248*, 2423–2434.
25. Yankowitz, M.; Xue, J. M.; Cormode, D.; Sanchez-Yamagishi, J. D.; Watanabe, K.; Taniguchi, T.; Jarillo-Herrero, P.; Jacquod, P.; LeRoy, B. J. Emergence of Superlattice Dirac Points in Graphene on Hexagonal Boron Nitride. *Nat. Phys.* **2012**, *8*, 382–386.
26. Kim, D.; Sun, D. Z.; Lu, W. H.; Cheng, Z. H.; Zhu, Y. M.; Le, D.; Rahman, T. S.; Bartels, L. Toward the Growth of an Aligned Single-Layer MoS_2 Film. *Langmuir* **2011**, *27*, 11650–11653.
27. Kibsgaard, J.; Lauritsen, J. V.; Clausen, B. S.; Topsøe, H.; Besenbacher, F. Cluster-Support Interactions and Morphology of MoS_2 Nanoclusters in a Graphite-Supported Hydrotreating Model Catalyst. *J. Am. Chem. Soc.* **2006**, *128*, 13950–13958.
28. Kibsgaard, J.; Clausen, B. S.; Topsøe, H.; Lægsgaard, E.; Lauritsen, J. V.; Besenbacher, F. Scanning Tunneling Microscopy Studies of TiO_2-Supported Hydrotreating Catalysts: Anisotropic Particle Shapes by Edge-Specific MoS_2-Support Bonding. *J. Catal.* **2009**, *263*, 98–103.
29. Gong, C.; Huang, C.; Miller, J.; Cheng, L.; Hao, Y.; Cobden, D.; Kim, J.; Ruoff, R. S.; Wallace, R. M.; Cho, K.; *et al.* Metal Contacts on Physical Vapor Deposited Monolayer MoS_2. *ACS Nano* **2013**, *7*, 11350–11357.

30. Walton, A. S.; Lauritsen, J. V.; Topsøe, H.; Besenbacher, F. MoS_2 Nanoparticle Morphologies in Hydrodesulfurization Catalysis Studied by Scanning Tunneling Microscopy. *J. Catal.* **2013**, *308*, 306–318.
31. Tuxen, A.; Kibsgaard, J.; Gøbel, H.; Lægsgaard, E.; Topsøe, H.; Lauritsen, J. V.; Besenbacher, F. Size Threshold in the Dibenzothiophene Adsorption on MoS_2 Nanoclusters. *ACS Nano* **2010**, *4*, 4677–4682.
32. Lauritsen, J. V.; Kibsgaard, J.; Helveg, S.; Topsøe, H.; Clausen, B. S.; Besenbacher, F. Size-Dependent Structure of MoS_2 Nanocrystals. *Nat. Nanotechnol.* **2007**, *2*, 53–58.
33. Helveg, S.; Lauritsen, J. V.; Lægsgaard, E.; Stensgaard, I.; Nørskov, J. K.; Clausen, B. S.; Topsøe, H.; Besenbacher, F. Atomic-Scale Structure of Single-Layer MoS_2 Nanoclusters. *Phys. Rev. Lett.* **2000**, *84*, 951–954.
34. Christensen, A.; Ruban, A. V.; Stoltze, P.; Jacobsen, K. W.; Skriver, H. L.; Nørskov, J. K.; Besenbacher, F. Phase Diagrams for Surface Alloys. *Phys. Rev. B: Condens. Matter Mater. Phys.* **1997**, *56*, 5822–5834.
35. Grey, F.; Bohr, J. A Symmetry Principle for Epitaxial Rotation. *Europhys. Lett.* **1992**, *18*, 717–722.
36. Barth, J. V.; Brune, H.; Ertl, G.; Behm, R. Scanning Tunneling Microscopy Observations on the Reconstructed Au(111) Surface: Atomic Structure, Long-Range Superstructure, Rotational Domains, and Surface Defects. *Phys. Rev. B: Condens. Matter Mater. Phys.* **1990**, *42*, 9307–9317.
37. Stradi, D.; Barja, S.; Diaz, C.; Garnica, M.; Borca, B.; Hinarejos, J. J.; Sanchez-Portal, D.; Alcami, M.; Arnau, A.; de Parga, A. L. V.; *et al.* Lattice-Matched *versus* Lattice-Mismatched Models to Describe Epitaxial Monolayer Graphene on Ru(0001). *Phys. Rev. B: Condens. Matter Mater. Phys.* **2013**, *88*, 245401.
38. Merte, L. R.; Grabow, L. C.; Peng, G.; Knudsen, J.; Zeuthen, H.; Kudernatsch, W.; Porsgaard, S.; Lægsgaard, E.; Mavrikakis, M.; Besenbacher, F. Tip-Dependent Scanning Tunneling Microscopy Imaging of Ultrathin Feo Films on Pt(111). *J. Phys. Chem. C* **2011**, *115*, 2089–2099.
39. Voloshina, E. N.; Fertitta, E.; Garhofer, A.; Mittendorfer, F.; Fonin, M.; Thissen, A.; Dedkov, Y. S. Electronic Structure and Imaging Contrast of Graphene Moire on Metals. *Sci. Rep.* **2013**, *3*, 1072.
40. Mattila, S.; Leiro, J. A.; Heinonen, M.; Laiho, T. Core Level Spectroscopy of MoS_2. *Surf. Sci.* **2006**, *600*, 5168–5175.
41. Lince, J. R.; Carre, D. J.; Fleischauer, P. D. Schottky-Barrier Formation on a Covalent Semiconductor without Fermi-Level Pinning—the Metal-MoS_2(0001) Interface. *Phys. Rev. B: Condens. Matter Mater. Phys.* **1987**, *36*, 1647–1656.
42. Shi, Y.; Huang, J.-K.; Jin, L.; Hsu, Y.-T.; Yu, S. F.; Li, L.-J.; Yang, H. Y. Selective Decoration of Au Nanoparticles on Monolayer MoS_2 Single Crystals. *Sci. Rep.* **2013**, *3*, 1634.
43. Monch, W. Valence-Band Offsets and Schottky Barrier Heights of Layered Semiconductors Explained by Interface-Induced Gap States. *Appl. Phys. Lett.* **1998**, *72*, 1899–1901.
44. Fontana, M.; Deppe, T.; Boyd, A. K.; Rinzan, M.; Liu, A. Y.; Paranjape, M.; Barbara, P. Electron-Hole Transport and Photovoltaic Effect in Gated MoS_2 Schottky Junctions. *Sci. Rep.* **2013**, 3.
45. Weber, T.; Muijsers, J. C.; Niemantsverdriet, J. W. Structure of Amorphous MoS_3. *J. Phys. Chem.* **1995**, *99*, 9194–9200.
46. Chaudhuri, A.; Lerotholi, T. J.; Jackson, D. C.; Woodruff, D. P.; Dhanak, V. Local Methylthiolate Adsorption Geometry on Au(111) from Photoemission Core-Level Shifts. *Phys. Rev. Lett.* **2009**, *102*, 126101.
47. Tsai, C.; Abild-Pedersen, F.; Nørskov, J. K. Tuning the MoS_2 Edge-Site Activity for Hydrogen Evolution *via* Support Interactions. *Nano Lett.* **2014**, *14*, 1381–1387.
48. Stroscio, J. A.; Kaiser, W. J. *Scanning Tunneling Microscopy*; Academic Press: San Diego, 1993; Vol. 27.
49. Zhang, C.; Johnson, A.; Hsu, C.-L.; Li, L.-J.; Shih, C.-K. Direct Imaging of Band Profile in Single Layer MoS_2 on Graphite: Quasiparticle Energy Gap, Metallic Edge States, and Edge Band Bending. *Nano Lett.* **2014**, *14*, 2443–2447.
50. Tersoff, J.; Hamann, D. R. Theory of the Scanning Tunneling Microscope. *Phys. Rev. B: Condens. Matter Mater. Phys.* **1985**, *31*, 805–813.
51. Kibsgaard, J.; Tuxen, A.; Knudsen, K. G.; Brorson, M.; Topsøe, H.; Lægsgaard, E.; Lauritsen, J. V.; Besenbacher, F. Comparative Atomic-Scale Analysis of Promotional Effects by Late 3d-Transition Metals in MoS_2 Hydrotreating Catalysts. *J. Catal.* **2010**, *272*, 195–203.